Available online at www.sciencedirect.com
ScienceDirect
Physica E 37 (2007) 81–87
PHYSICA E
www.elsevier.com/locate/physe

Raman scattering from one-dimensional carbon systems

M.S. Dresselhaus[a,b,*], F. Villalpando-Paez[c], Ge.G. Samsonidze[a], S.G. Chou[c], G. Dresselhaus[d], J. Jiang[e], R. Saito[e], A.G. Souza Filho[g], A. Jorio[b,f], M. Endo[h], Y.-A. Kim[h]

[a]*Department of Electrical Engineering and Computer Science, Massachusetts Institute of Technology, Cambridge, MA 02139-4307, USA*
[b]*Department of Physics, Massachusetts Institute of Technology, Cambridge, MA 02139-4307, USA*
[c]*Department of Chemistry, Massachusetts Institute of Technology, Cambridge, MA 02139-4307, USA*
[d]*Francis Bitter Magnet Laboratory, Massachusetts Institute of Technology, Cambridge, MA 02139-4307, USA*
[e]*Department of Physics, Tohoku University and CREST, JST, Sendai 980-8578, Japan*
[f]*Departamento de Física, Universidade Federal de Minas Gerais, Belo Horizonte, MG 30123-970, Brazil*
[g]*Departamento de Física, Universidade Federal do Ceará, 60455-900 Fortaleza, Ceará, Brazil*
[h]*Faculty of Engineering, Shinshu University 4-17-1 Wakasato, Nagano-shi 380-8553, Japan*

Available online 15 December 2006

Abstract

Although the Raman effect was discovered nearly 80 years ago, it is only recently that the special characteristics of Raman scattering for one-dimensional systems have been seriously considered. This review focuses on the special interest of the Raman effect for one-dimensional systems that is of particular relevance to carbon nanostructures. Two examples of Raman scattering in one-dimensional systems are given. The first illustrates the use of Raman spectroscopy to reveal the remarkable structure and properties of carbon nanotubes arising from their one-dimensionality. Some of the recent advances in using Raman spectroscopy to study doping and intercalation to modify nanotube properties are reviewed, in the context of a one-dimensional system. The second example is the Raman spectra of a linear chain of carbon atoms and the special properties of this interesting system. New approaches toward applying Raman spectroscopy to carbon nanostructures are also emphasized.

PACS: 78.67.Ch; 78.30.Na; 73.22.−f; 78.55.−m; 71.35.−y

Keywords: Raman spectroscopy; One-dimensional systems; Carbon nanostructures; Carbon nanotubes

1. Introduction

Photo-physics probes such as Raman spectroscopy, which have historically provided sensitive, easily available and non-destructive techniques for characterizing 3D graphites and 2D sp^2 carbons, are now providing powerful tools both for the characterization of one-dimensional (1D) carbon systems and for the discovery and exploration of new phenomena occurring in such systems. Single wall carbon nanotubes have provided an ideal system for the development of the field of 1D Raman scattering because their very small diameters (~1 nm) and their long lengths (~100 μm) lead to very high aspect ratios with length to diameter ratios of $\sim 10^5$, thereby establishing their strong one-dimensionality.

2. Raman spectroscopy of 1D carbon nanotubes

The important breakthrough in the study of 1D Raman spectroscopy occurred in 2001 [1] when it was shown that Raman spectra could be observed from individual (n,m) semiconducting and metallic carbon nanotubes because of the strong resonance Raman process that is observed for a 1D system only 1 nm in diameter. Here (n,m) are two integer indices used to characterize the structure of every unique carbon nanotube, where the chiral vector $\vec{C}_h$ which forms the circumference of every single wall carbon nanotube is given by $\vec{C}_h = n\vec{a}_1 + m\vec{a}_2$ where $\vec{a}_1$ and $\vec{a}_2$ are

*Corresponding author. Department of Electrical Engineering and Computer Science, Massachusetts Institute of Technology, Cambridge, MA 02139-4307, USA. Tel.: +1 617 253 6864; fax: +1 617 253 6827.
E-mail address: millie@mgm.mit.edu (M.S. Dresselhaus).

1386-9477/$ - see front matter © 2006 Published by Elsevier B.V.
doi:10.1016/j.physe.2006.07.048

the unit cell basis vectors of the graphene sheet, constituting a single layer plane of 3D graphite. It was further shown that each (n,m) nanotube has a unique Raman spectrum [1], because the trigonal warping effect [2] yields distorted constant energy contours with threefold symmetry around the K point in the 2D graphite Brillouin zone. The cutting lines associated with each (n,m) single wall nanotube (SWNT) thus produce a unique set of van Hove singularities and therefore a unique Raman spectrum [3]. Since the radial breathing mode (RBM) frequencies in the Raman spectra of SWNTs are directly related to the nanotube diameters d_t, and since the resonance Raman scattering (RRS) process is highly selective of individual (n,m) nanotubes, the tube diameter and the optical transition energy E_{ii} can be used to determine the (n,m) indices of individual tubes [4].

The advent of single nanotube Raman spectroscopy and the ability to measure spectra on each (n,m) nanotube allowed the investigation of properties of carbon systems that were not previously accessible, such as the study of electron and phonon dispersion relations as a function of wave vector direction [3,5,6], and the study of the diameter and chiral angle dependence of each of the spectral features observed in the resonant Raman spectra for carbon nanotubes. These Raman features include the RBM, the G-band features, the intermediate frequency modes, the D-band, the G'-band and other higher-order Raman features [7]. By summing the results over a range of diameters and chiral angles, it becomes possible to reconstruct spectra observed for samples containing ensembles of tubes that have various diameter distributions. The combination of Raman spectroscopy measurements together with other techniques, such as transport measurements, provided a means to measure the chirality and diameter dependence of many nanotube properties [8,9].

A second breakthrough in the photo-physics of SWNTs occurred when it was discovered that by wrapping SWNTs with sodium dodecyl sulfate (SDS), photoexcited isolated semiconducting nanotubes in solution could remain in excited states long enough to produce a PL signal with an emission energy and an $(n-m)$ family behavior that could also be used for their (n,m) determination [10,11]. This breakthrough led to PL experiments on many (~33) SDS wrapped SWNTs in solution in a single experiment. In these experiments the excitation energy was at E_{22} for a particular tube followed by subsequent emission at an energy E_{11}. By noting the $(n-m)$, $(2n+m)$ and $(2m+n)$ family behavior, these authors were able to identify individual (n,m) tubes with specific E_{22}^S absorption peaks and specific E_{11}^S emission peaks for semiconducting SWNTs produced by the HiPco process (diameter distribution $d_t = 1.05 \pm 0.15$ nm). Initially these PL measurements on SDS wrapped HiPco tubes in solution were compared with RRS measurements on isolated SWNTs with much larger diameter ($d_t = 1.5 \pm 0.2$ nm) sitting on a Si/SiO_2 substrate. For the RRS measurements, the resonance between the laser excitation energy E_{laser} and the nanotube van Hove singularities associated with the 1D density of states occurred for the E_{33}^S, E_{44}^S, and E_{11}^M interband transitions where no clear family effects were observed, and the ratio E_{44}^S/E_{33}^S for specific SWNTs appeared to follow the simple tight binding model [1]. In contrast, the PL spectra yielded E_{22}^S/E_{11}^S ratios for specific (n,m) tubes which differed strongly from the simple tight binding model prediction, and showed very different family effects for type 1 and type 2 semiconducting tubes, where families with $2n+m = 3p+1$ (or $3p+2$) correspond to type 1 (or type 2) semiconducting SWNTs, and p is an integer. To demonstrate that the same physical model could explain both types of photo-physical experiments, RRS and PL experiments were carried out on the same physical SDS wrapped HiPco sample, yielding consistent values for both the E_{ii}^S transitions and (n,m) identifications [12]. To put the interpretation of these photo-physical spectra on a firmer theoretical basis, an extended tight binding (ETB) calculation was carried out, which included curvature effects (that are important for small diameter SWNTs), long range interactions, and geometrical structure optimization to allow for atomic relaxation to equilibrium positions on a curved surface [6]. Many body effects were semi-empirically incorporated into the ETB model. As seen in Fig. 1(a), the ETB model shows a strong $(2n+m, \text{mod } 3)$ family behavior, with a different behavior observed for type 1 and type 2 semiconducting SWNTs.

The ability of PL to yield the transition energies E_{ii} at once for many (n,m) SDS wrapped nanotubes in solution led to the development of Raman techniques based on the use of many laser lines to map out Raman intensity contours on a plot of laser excitation energy vs. Raman frequency, such as that shown in Fig. 1(b) [12]. Maps of Raman intensities have subsequently been used to show a variety of other physical phenomena, such as highlighting the spatial dependence of structural defects or strain effects in SWNTs.

Another important recent advance in nanotube photophysics relates to the use of different nanotube wrapping agents, initially introduced for the purpose of nanotube isolation in PL experiments. DNA provides another nanotube wrapping agent that has been shown to be rather effective in (n,m) SWNT separation, as shown in the RRS spectra in Fig. 2(a). Nanotubes produced by the CoMoCAT process yielding SWNTs in the diameter range $d_t = 0.81 \pm 0.05$ nm showed a large reduction in the number of *metallic* nanotubes in the sample after going through an ion exchange chromatography column [13,14]. A sample with a large concentration of (6,5) SWNTs could thus be obtained, as shown in the resonance Raman spectra in Fig. 2(a). Measurements of such samples further showed that the RBM frequency for an (n,m) SWNT is not much different between SDS and DNA wrapped samples, and between wrapped and pristine samples, though the transition energies E_{ii} can shift by significant amounts (~30 meV) compared with the width of the

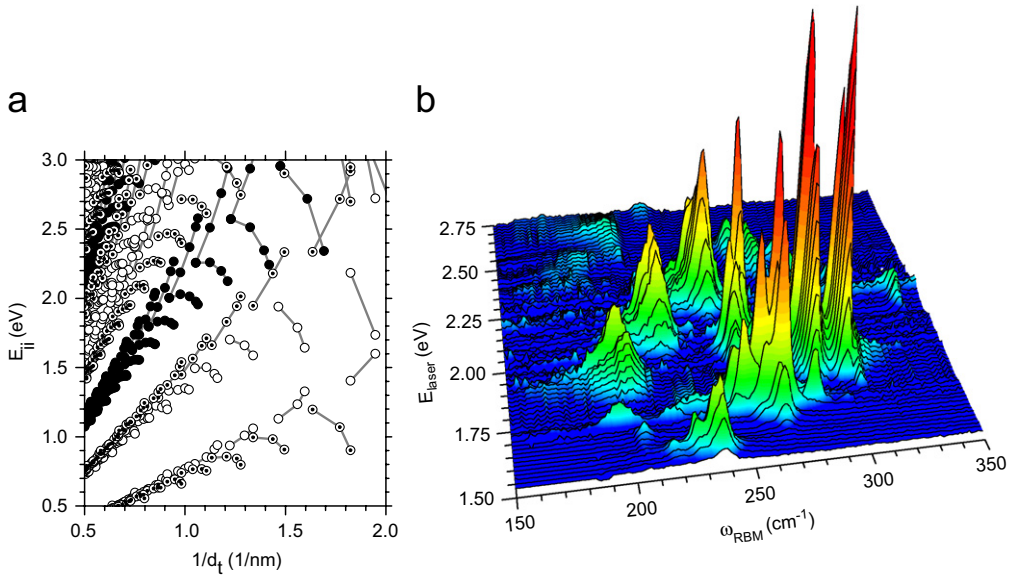

Fig. 1. (a) "Kataura" plot of transition energies E_{ii} vs. inverse diameter $1/d_t$ for metallic (solid dots), semiconducting type 1 (open dots) and type 2 (marked dots) SWNTs based on the extended tight binding (ETB) model using the $(2n+m, \text{mod } 3)$ definition of type 1 and type 2 semiconducting tubes (see text) [6]. (b) RBM resonant Raman measurements with 76 different laser lines of HiPco carbon nanotubes dispersed an aqueous solution of SDS wrapped SWNTs where the E_{ii} of RRS and PL are compared on the same tubes [12].

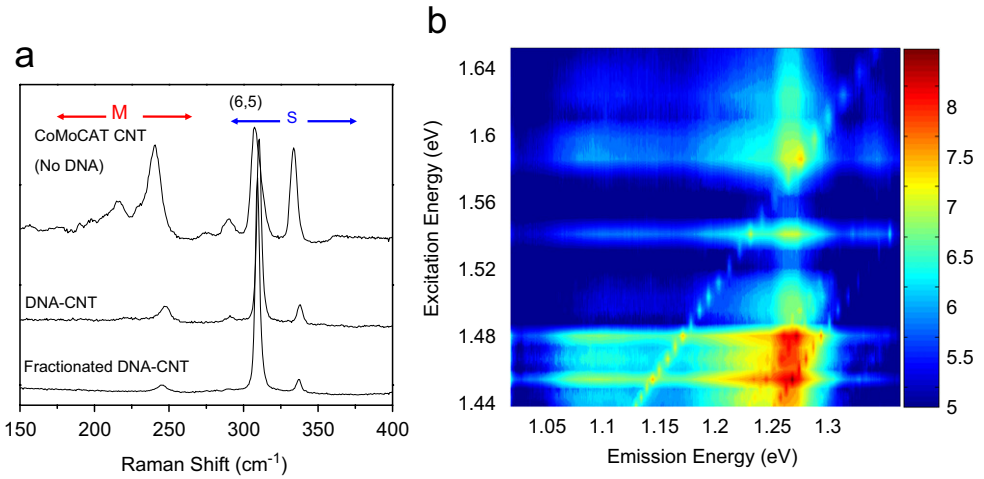

Fig. 2. (a) Raman spectra of different DNA-wrapped CoMoCAT carbon nanotube samples taken with 2.18 eV laser excitation energy. After separation using ion exchange chromatography, the fractionated DNA-CNT sample became enriched with the (6, 5) nanotube [13]. (b) A 2D excitation vs. emission photoluminescence contour map for a dried (6, 5) enriched DNA-CNT sample on a sapphire substrate. The spectral intensity is plotted using the log scale shown on the right [15].

resonance window for dried DNA wrapped SWNT samples (~15 meV) that were measured [13].

The availability of a sample with a very large concentration of a single (n, m) species allows interesting new photophysics studies to be carried out. Thus using a (6,5) enriched DNA wrapped SWNT sample obtained after ion exchange chromatography, it has been possible by use of RRS and PL measurements to identify specific SWNT phonon-assisted absorption mechanisms, specific phonon-assisted emission processes, and specific Raman-assisted processes [15]. Such a detailed identification is possible since the nanotube selects specific energies and wave vectors through the presence of van Hove singularities in SWNTs and the requirements of energy-momentum conservation in first-order and double resonance processes. Fig. 2(b) shows PL experiments in the frequency domain [15], illustrating the physical processes enumerated above. Related experiments on the same sample have also been carried out in the time domain [16] to study the dynamics of these phonon related processes. Recent studies based on two photon absorption studies [17] have shown that the photo-physics of SWNTs is dominated by excitonic effects. Since the electronic structure $E(k)$ of carbon nanotubes is based on two degenerate bands with a linear E vs. k

relation, four distinct types of excitons are needed to describe the photo-physics of carbon nanotubes in contrast to the situation for common semiconductors where only one type of exciton is sufficient. Of the four types of excitons which exist in SWNTs, only one type is optically active, leading to one bright exciton and three dark excitons. At present, much effort is going into trying to understand the bright and dark excitonic states and their relation to the band states lying about 0.4 eV higher in energy in the case of SWNTs with $d_t \leqslant 1$ nm.

3. Intercalation in 1D systems

Intercalation is a method to introduce guest species between the atomic layers of a host material to modify the properties of that system in a controllable way. In this context intercalation has provided a key method for the controlled modification of the properties of graphite by introducing guest species between the layers of graphite thereby exploiting its strong in-plane bonding and very weak interplanar bonding. Graphite intercalation compounds have provided a model system for studying many aspects of 2D electrons and phonons and these studies have also contributed to our understanding of 2D Raman spectroscopy [18,19]. Intercalation has recently been applied to bundles of carbon nanotubes, and as expected the results bear many similarities to their graphite intercalation compound analog, but also many differences. One particularly informative system has been the intercalation of bromine into double wall carbon nanotubes (DWNTs) [20] because this system allows the observation of the Raman spectra from both the host carbon and from the guest Br_2 species [18]. Such observations have allowed us to get additional insights when studying the charge transfer between the dopant and the host DWNTs. The use of different laser lines allowed us to study different configurations of metallic (M) and semiconducting (S) outer/inner tubes separately, such as M/S and S/M outer/inner tube configurations. By using a sample with small diameter tubes, it has been possible to study the effects of doping on the individual $2n + m$ families and to identify the specific (n, m) tubes that are resonant in each spectrum. For example with $E_{laser} = 1.96$ eV we can probe in great detail the inner nanotubes which are metallic, while at $E_{laser} = 1.58$ eV we can probe the case where the inner tubes are metallic and the outer tubes are semiconducting opposite to the case of $E_{laser} = 2.33$ eV where we probe inner tubes that are semiconducting and outer tubes that are metallic. Therefore intercalation studies provide a very sensitive tool for studying a wide variety of intercalation effects in DWNTs, not present in graphite intercalation compounds. The 1D alignment of the intercalated species in DWNT samples is another effect that is unique about nanotube intercalation relative to its 3D counterpart.

Fig. 3(a)–(d) shows TEM and SEM images of the double wall tubes before and after bromination showing that the tubes survive very well through multiple intercalation cycles. Both decreases and increases in the RBM intensity due to bromination are observed. An example of a decrease in the RBM frequencies through bromination can be seen in Fig. 3(e) which shows many Raman spectra taken in the RBM frequency range as the temperature is increased to release the bromine and then as the sample temperature is decreased again to room temperature. We have also

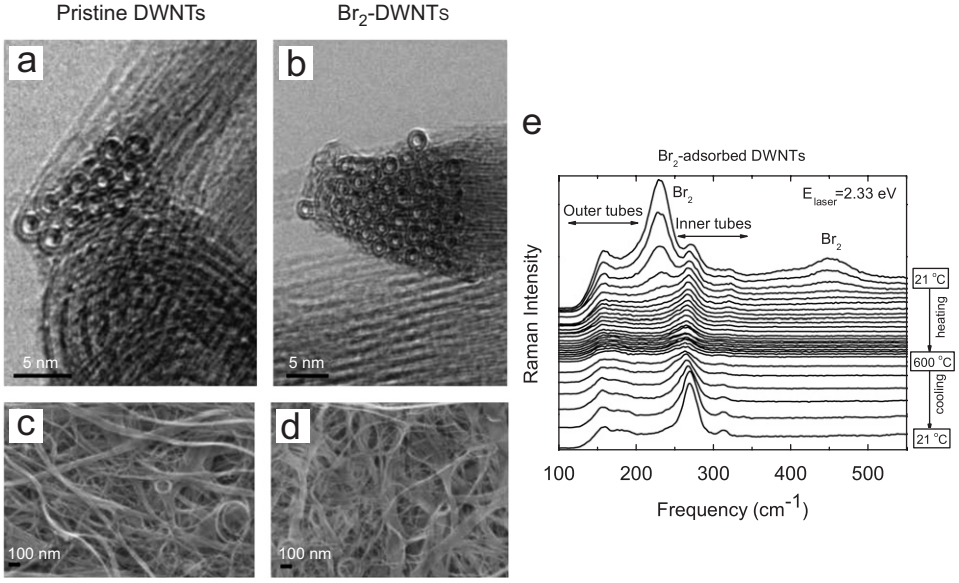

Fig. 3. Transmission electron microscope (TEM) images of pristine double wall carbon nanotubes (a) before and (b) after Br_2 adsorption; (c) and (d) show, respectively, the corresponding scanning electron microscope (SEM) images, for both pristine and Br_2-doped DWNTs. (e) In situ Raman spectra of Br_2-adsorbed DWNTs subjected to different thermal annealing temperatures during heating (in steps of 25 °C) and cooling (in steps of 100 °C). The Raman spectra were excited by $E_{laser} = 2.33$ eV [20].

observed the resonance spectra from DWNTs for which E_{laser} is in resonance with $E_{11}^{M}(H)$, the higher energy van Hove singularity for metallic nanotubes, a virtually unexplored phenomenon because of the small magnitude of the electron-phonon matrix elements for these transitions compared to resonances with the lower energy van Hove singularity $E_{11}^{M}(L)$ that is traditionally observed. The S/S configuration was also studied and relatively large shifts in the transition energy E_{22}^{S} were observed for this small diameter tube. Furthermore, we have found that Br_2 molecules interact with the DWNTs and their intercalation and de-intercalation are completely reversible upon thermal annealing at 600 °C. Upshifts in the Raman frequencies for the tangential modes and depression of their Raman intensities indicated that electrons are transferred from the nanotubes to the Br_2 molecules. Metallic nanotubes are specially sensitive to the adsorption of Br_2 molecules, even when they are the inner tubes of DWNTs.

Upon heating, we can observe that the mode at 233 cm^{-1} and its overtone at 460 cm^{-1}, which are assigned to the Br_2 molecular vibrations, gradually lose intensity with increasing heat treatment temperature, disappearing completely at an annealing temperature of 225 °C. After cooling down to room temperature, we can observe that the RBM spectrum for our samples exhibits slight changes for the outer tubes. The modes close to 270 cm^{-1} which are for metallic inner tubes are somewhat enhanced in the pristine sample relative to the intercalated sample, and a similar effect is also found for the semiconducting inner tube at ~310 cm^{-1}. The outer tubes that are resonant at E_{laser} = 2.33 eV are semiconducting tubes and these are well resolved both for the brominated and pristine samples. Unlike the situation in bromine-intercalated graphite where some bromine intercalant remains after heat treatment, the removal of bromine for DWNT intercalation is reversible and the initial Raman spectra observed before bromine doping are recovered after heating the intercalated DWNTs to 225 °C (see Fig. 3(e)).

4. Linear carbon chains

A number of vibrational modes are traditionally observed in the Raman spectra for SWNT and DWNTs and in graphite above the maximum frequency of 1620 cm^{-1} in the first-order graphite Raman spectra and in the frequency range of 1700–2000 cm^{-1}. For isolated tubes and SWNT bundles, the Raman spectra show a set of double resonance modes (M^- and M^+) associated with the oTO phonon that is infrared active in graphite. In addition a highly dispersive double resonance combination mode (iTOLA) is observed, reflecting the strong dispersion of the longitudinal acoustic (LA) mode and the much weaker dispersion of the iTO mode of graphite. Under some circumstances, another mode in this general frequency range, but with rather different physical characteristics, has been reported at ~1850 cm^{-1} [21]. By studying this ~1850 cm^{-1} feature in the Raman spectra of DWNTs as a function of heat treatment temperature (see Fig. 4), it has been possible to study the coalescence process in DWNTs and in so doing we have been able to study, by using Raman spectroscopy, the role of short linear carbon chains in the DWNT coalescence process.

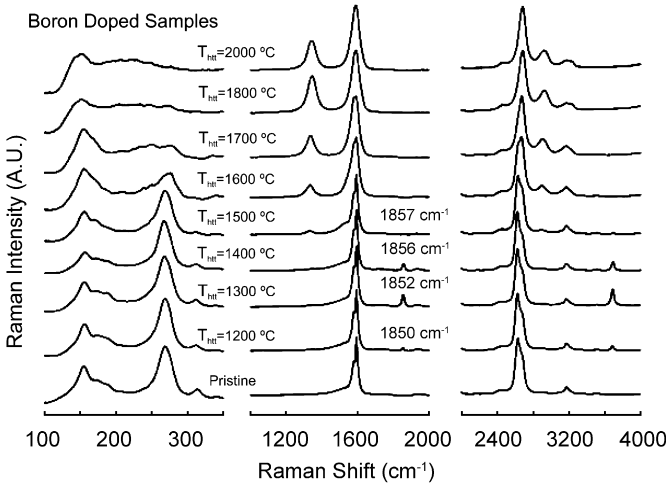

Fig. 4. Raman spectra taken at 2.33 eV on the boron doped DWNT samples, as prepared (pristine) and heated to various heat treatment temperatures (T_{htt}) with special emphasis given to the CIM feature at 1850–1857 cm^{-1} range and its harmonic near 3690 cm^{-1}.

Upon heat treatment to T_{htt} = 1300 °C, a weak Raman feature appears at ~1850 cm^{-1} as the RBM intensity of the smallest diameter inner tube starts to decrease. The effect of heat treatment can be seen visually in the HRTEM images taken on the same samples as were used for this Raman study. The HRTEM images of the DWNTs with T_{htt} = 1500 °C clearly show signs of tube coalescence [22] and for this reason the ~1850 cm^{-1} feature is called the coalescence inducing mode (CIM).

In Fig. 4 we see Raman spectra for boron doped DWNTs heat treated to various heat treatment temperatures T_{htt} [22]. In this figure we see that the presence of boron promotes the development of the 1850 cm^{-1} feature at lower T_{htt}, as compared to the case without boron doping of the DWNTs. Furthermore the CIM peak for the boron doped samples reaches a maximum intensity at T_{htt} = 1300 °C, and then decreases in intensity as coalescence of the smaller diameter tubes starts to appear strongly in the HRTEM images taken from the T_{htt} = 1400 °C sample. The relative intensities for the first-order Raman CIM peak and its second harmonic at 3690 cm^{-1} are strongly coupled to each other with very little change in the mode frequency upon doping at constant T_{htt}. Since this peak shows no dispersion with E_{laser} [23], we conclude that the CIM feature is a first-order Raman effect. Studies of the dependence of the CIM intensity on E_{laser} show a dominant maximum at ~2.23 eV, which is identified with the electronic energy associated with these linear chains [23]. Calculations show that the linear carbon chains that promote coalescence are short (~5 carbon atoms long) and they bond preferentially to adjacent tubes. As T_{htt}

increases, their intensity decreases as they are consumed by the tube coalescence process [22].

As the maximum intensity of the CIM is reached, the RBM intensities of the smaller diameter inner and outer pair of a DWNT start to decrease, while the disorder-induced modes (such as the D-band and the $D+G$ combination mode at $2950\,\mathrm{cm}^{-1}$) start to increase in intensity. By the time $T_{\mathrm{htt}} = 1500\,^{\circ}\mathrm{C}$ is reached, the HRTEM images show several major changes: (1) widespread nanotube coalescence, (2) widespread conversion of DWNTs to large diameter disordered SWNTs, (3) the initiation of regions of non-nanotube sp^2 carbonaceous material, and (4) the strong development of the D-band and the $D+G$ combination modes. Since the CIM mode is observed in highly purified DWNTs heat treated in pure argon gas that show beautiful TEM images, we conclude that the CIM feature involves only carbon atoms and this conclusion is also in agreement with prior observations [21]. Boron plays a role in catalyzing the coalescence process so that it occurs much more strongly and at lower temperatures, and boron also helps to bond the carbon chains to the nanotubes. When the coalescence process occurs, these short chains become incorporated into the large diameter tubes along with some of the boron atoms, thereby contributing to the growth of the D-band. Coalescence of DWNTs also occurs with heat treatment, but in the pristine case no D-band is seen in the Raman spectra. From this study we see how Raman spectroscopy provides a wealth of information about linear chains of carbon atoms and about their role in the coalescence process of DWNTs.

5. Conclusions

In the last few years single tube resonance Raman and photoluminescence experiments have made it possible to determine the unique (n,m) structure of one-dimensional systems like carbon nanotubes. Furthermore, our recent ability to use surfactants and wrapping agents to separate nanotubes allowing measurement of their (n,m) indices has enabled widespread studies of the chirality dependence of the physical properties of carbon nanotubes.

Because of the potential importance of DWNTs and the doping of carbon nanotubes [24] for practical applications, we can expect these types of nanotubes to receive increased attention in the future. The possible metallic or semiconducting configurations (M/S, S/S, etc.) that a DWNT sample can have provide an excellent platform to study the differences between metallic and semiconducting tubes and the interaction of nanotubes with dopants and intercalants. The use of tunable lasers and doped samples with different amounts of dopant and charge transfer will allow researchers to do very detailed studies of the doping effects on nanotubes and will elucidate the differences and similarities between nanotubes and graphite or the similarities and differences between 1D and 2D carbon systems. Furthermore, such studies will allow us to distinguish between the contributions of dopants and intercalants to shifting the Fermi energy and to shifting the optical transition energies themselves.

The potential benefits of incorporating nanotubes into microelectronic devices will continue to stimulate investigations aimed at producing a sample that contains only one certain kind of (n,m) nanotube. In this context, doping, intercalation and defect engineering are likely to provide the necessary means to fine tune the electronic and mechanical structure of nanotubes. Due to their highly reactive nature, sp carbon chains are somewhat difficult to observe but Raman spectroscopy has now been shown to provide a useful tool to study their behavior. Recent advances in the study of these 1D structures in the DWNT coalescence process are expected to aid the study of sp bonded carbon in a variety of other carbon systems where 1D carbon chains may form.

Acknowledgments

MIT authors acknowledge support under NSF Grant DMR 04-05538, R.S. acknowledges a Grant-in-Aid (No. 16076201) from the Ministry of Education, Japan, and A.J. acknowledges financial support from CNPq and FAPEMIG, Brazil. F. Villalpando-Paez is grateful to CONACYT Mexico, SEP Mexico and Grupo Jumex for financial support.

References

[1] A. Jorio, R. Saito, J.H. Hafner, C.M. Lieber, M. Hunter, T. McClure, G. Dresselhaus, M.S. Dresselhaus, Phys. Rev. Lett. 86 (2001) 1118.
[2] R. Saito, G. Dresselhaus, M.S. Dresselhaus, Phys. Rev. B 61 (2000) 2981.
[3] G.G. Samsonidze, R. Saito, A. Jorio, M.A. Pimenta, A.G. Souza Filho, A. Grüneis, G. Dresselhaus, M.S. Dresselhaus, J. Nanosci. Nanotechnol. 3 (2003) 431.
[4] M.S. Dresselhaus, G. Dresselhaus, A. Jorio, A.G. Souza Filho, R. Saito, Carbon 40 (2002) 2043.
[5] G.G. Samsonidze, R. Saito, A. Jorio, A.G. Souza Filho, A. Grüneis, M.A. Pimenta, G. Dresselhaus, M.S. Dresselhaus, Phys. Rev. Lett. 90 (2003) 027403.
[6] G.G. Samsonidze, R. Saito, N. Kobayashi, A. Grüneis, J. Jiang, A. Jorio, S.G. Chou, G. Dresselhaus, M.S. Dresselhaus, Appl. Phys. Lett. 85 (2004) 5703.
[7] M.S. Dresselhaus, G. Dresselhaus, R. Saito, A. Jorio, Phys. Rep. 409 (2005) 47.
[8] S.B. Cronin, A.K. Swan, M.S. Ünlü, B.B. Goldberg, M.S. Dresselhaus, M. Tinkham, Phys. Rev. Lett. 93 (2004) 167401.
[9] A.G. Souza Filho, N. Kobayasi, J. Jiang, A. Grüneis, R. Saito, S.B. Cronin, J. Mendes Filho, G.G. Samsonidze, G. Dresselhaus, M.S. Dresselhaus, Phys. Rev. Lett. 95 (2005) 217403.
[10] M.J. O'Connell, S.M. Bachilo, X.B. Huffman, V.C. Moore, M.S. Strano, E.H. Haroz, K.L. Rialon, P.J. Boul, W.H. Noon, C. Kittrell, J. Ma, R.H. Hauge, R.B. Weisman, R.E. Smalley, Science 297 (2002) 593.
[11] S.M. Bachilo, M.S. Strano, C. Kittrell, R.H. Hauge, R.E. Smalley, R.B. Weisman, Science 298 (2002) 2361.
[12] C. Fantini, A. Jorio, M. Souza, M.S. Strano, M.S. Dresselhaus, M.A. Pimenta, Phys. Rev. Lett. 93 (2004) 147406.

[13] S.G. Chou, H.B. Ribeiro, E. Barros, A.P. Santos, D. Nezich, G.G. Samsonidze, C. Fantini, M.A. Pimenta, A. Jorio, F. Plentz Filho, M.S. Dresselhaus, G. Dresselhaus, R. Saito, M. Zheng, G.B. Onoa, E.D. Semke, A.K. Swan, M.S. Ünlü, B.B. Goldberg, Chem. Phys. Lett. 397 (2004) 296.
[14] M. Zheng, A. Jagota, M.S. Strano, P. Barone, S.G. Chou, B.A. Diner, M.S. Dresselhaus, R.S. McLean, G.B. Onoa, A.P. Santos, E.D. Semke, M. Usrey, D.J. Walls, Science 302 (2003) 1545.
[15] S.G. Chou, F. Plentz Filho, J. Jiang, R. Saito, D. Nezich, H.B. Ribeiro, A. Jorio, M.A. Pimenta, G.G. Samsonidze, A.P. Santos, M. Zheng, G.B. Onoa, E.D. Semke, G. Dresselhaus, M.S. Dresselhaus, Phys. Rev. Lett. 94 (2005) 127402.
[16] S.G. Chou, M.F. DeCamp, J. Jiang, G.G. Samsonidze, E.B. Barros, F. Plentz Filho, A. Jorio, M. Zheng, G.B. Onoa, E.D. Semke, A. Tokmakoff, R. Saito, G. Dresselhaus, M.S. Dresselhaus, Phys. Rev. B 72 (2005) 195415.
[17] F. Wang, G. Dukovic, L.E. Brus, T.F. Heinz, Science 308 (2005) 838.
[18] M.S. Dresselhaus, G. Dresselhaus, Adv. Phys. 51 (2002) 1–186 reprinted from M.S. Dresselhaus, G. Dresselhaus, Adv. Phys. 30 (1981).
[19] M.S. Dresselhaus, P.C. Eklund, Adv. Phys. 49 (2000) 705.
[20] A.G. Souza Filho, M. Endo, H. Muramatsu, T. Hayashi, Y.A. Kim, E.B. Barros, N. Akuzawa, G.G. Samsonidze, R. Saito, M.S. Dresselhaus, Phys. Rev. B 73 (2006) 235413.
[21] Y. Zhao, Y. Ando, Y. Liu, M. Jisino, T. Suzuki, Phys. Rev. Lett. 90 (2003) 187401.
[22] M. Endo, M. Terrones, Y.A. Kim, T. Hayashi, H. Muramatsu, R. Saito, F. Villapando, S.G. Chou, M.S. Dresselhaus, Nanotube coalescence inducing mode: a novel vibrational mode in carbon systems, Small 2 (2006) 1031.
[23] C. Fantini, E. Cruz, A. Jorio, M. Terrones, H. Terrones, V. G, J.-C. Charlier, M.S. Dresselhaus, R. Saito, Y.A. Kim, T. Hayashi, H. Muramatsu, M. Endo, M.A. Pimenta, Phys. Rev. B 73 (2006) 193408.
[24] M. Terrones, A. Jorio, M. Endo, A.R. Rao, Y.A. Kim, T. Hayashi, H. Terrones, J.-C. Charlier, G. Dresselhaus, M.S. Dresselhaus, Mater. Today Mag. 7 (2004) 30.